### AN INVERSION INTEGRAL FOR CRACK-SCATTERING DATA

### J. D. ACHENBACH, K. VISWANATHAN\* and A. NORRIS

The Technological Institute, Northwestern University, Evanston, IL 60201, U.S.A.

Received 4 June 1979

The inverse problem of determining the size, shape and orientation of a flat crack from high-frequency far-field elastic waves scattered by the crack is investigated. The results show that desired information on a crack can be obtained from the first arriving scattered longitudinal waves only. It is shown that an approximate high-frequency solution to the direct problem, based on physical elastodynamics, yields an expression for the scattered far-field of longitudinal motion which suggests a solution to the inverse problem by application of Fourier-type inversion integrals to scattering data. Two kinds of inversion integrals are examined. The inversion problem becomes relatively simple if some a-priori information is available, either on the orientation of the plane of the crack or on a plane of symmetry. The method of inversion is verified for a flat crack of elliptical shape. Some computational technicalities are discussed, and the method is also applied to experimental scattering data.

#### 1. Introduction

An important method of crack detection is based on scattering of mechanical waves by cracks. The presence of a crack is relatively easy to detect. The determination of the size, shape and orientation from the scattered field poses, however, a difficult inverse scattering problem.

The work reported in this paper was motivated in part by the need for a method to locate hydraulically induced fractures in a hot-dry-rock geothermal energy system, see e.g. [1], and in part by methods of crack detection by ultrasonic waves in quantitative non-destructive evaluation of materials [2]. The practical difficulties in a geophysical setting are of course much greater than in a materials-testing situation. The additional difficulties stem from the more complicated and to some extent unknown mechanical behavior of the earth as well as from the more severe limitations on the placement of measuring equipment.

In experimental work on quantitative flaw definition either the pulse-echo method with one transducer or the pitch-catch method with two transducers is used. Most experimental setups include instrumentation to gate out and spectrum analyze the signal diffracted by a flaw. The raw scattering data generally need to be corrected for transducer transfer functions and other characteristics of the system, which have been obtained on the basis of appropriate calibrations. After processing, the information available ideally consists of the amplitude and the phase, albeit over a limited frequency range, and at a limited number of points of observation.

Insight into the solution to the direct scattering problem, that is, the computation of the field generated when a mechanical wave is diffracted by a known flaw, is a necessary preliminary to the inverse problem. From the theoretical point of view a flat crack is a planar surface across which the displacement can be discontinuous. The solution of direct elastodynamic scattering problems is rather complicated. Approximate methods to solve the scattering problem, especially in the high-frequency range, have been presented in Refs. [3] and [4]. In an exact formulation the direct problem is a mixed boundary value problem, which can be reduced to one or more generally singular integral equations for the displacement discontinuities

<sup>\*</sup> Permanent address: Defense Science Laboratory, Dehli-110054, India.

across the crack faces. For a crack of arbitrary shape this integral equation was derived by Budiansky and Rice [5].

There is a considerable literature on diffraction of plane waves by slits and penny-shaped cracks. Much of this work was recently summarized in a review article by Kraut [6]. Another review article was recently published by Datta [7]. A great deal of useful information, and an extensive list of references, is also contained in the book by Pao and Mow [8]. A comprehensive review of acoustic and electromagnetic scattering from discs and other simple shapes has been compiled by Bowman, Senior and Uslenghi [9]. Practical aspects, as well as analytical and experimental results on the application of elastic waves in the non-destructive testing of materials, have recently been discussed in Ref. [10].

In this paper we discuss the inversion of far-field crack-scattering data in the high-frequency range. For an acoustic medium inverse problems have been discussed by Lewis [11]. In recent years Cohen and Bleistein have made significant contributions to the inverse problem for cavities in acoustic media, see e.g. [12]. Surveys of recent work on related inverse problems can be found in Refs. [13, 14].

The analysis is for time-harmonic motions, but the term  $\exp(-i\omega t)$  is generally omitted. The equations governing elastodynamic theory relative to a system of Cartesian coordinates are stated in considerable detail in Ref. [15]. In a homogeneous, isotropic, linearly elastic solid the components of the stress tensor,  $\tau_{ii}(x)$ , are related to the gradients of the displacement components  $u_{i,j}(x)$  by

$$\tau_{ii} = \lambda u_{k,k} \delta_{ii} + \mu (u_{i,i} + u_{i,i}) \tag{1.1}$$

where  $\lambda$  and  $\mu$  are Lame's elastic constants. Substitution of this relation into the balance equation of linear momentum yields the displacement equations of motion

$$\mu u_{i,ii} + (\lambda + \mu)u_{i,ii} + \rho \omega^2 u_i = -F_i \tag{1.2}$$

where  $\rho$  is the mass density and  $F_i$  are the components of the body force distribution (per unit volume). These equations should be supplemented by

$$t_l = \tau_{kl} n_k. \tag{1.3}$$

At a surface S, Eq. (1.3) relates the components of the traction to the components of the stress tensor and the unit normal to S.

## 2. Scattering of high-frequency elastic waves

In this section we briefly review some pertinent elastodynamic theory, and we present an approximate solution to the direct scattering problems. This solution is for the far-field and in the high-frequency range, and it is concerned only with the scattered field of longitudinal motion.

#### 2.1. Basic singular solution

The three-dimensional basic elastodynamic singular solution for an unbounded domain is the solution to Eq. (1.2) when  $F_i(x)$  is of the form

$$F_i = f_i \delta(\mathbf{x} - \mathbf{X}), \tag{2.1}$$

i.e., when F is a unit point load applied at  $x_i = X_i$ , acting in the direction defined by the unit vector f. In this solution the components of  $u^G$  depend linearly on the components of f. To express this dependence we

introduce a tensor of rank two,  $u_{i;m}^G(\mathbf{x} - \mathbf{X})$ , and a tensor of rank three  $\tau_{ij;m}^G(\mathbf{x} - \mathbf{X})$ , which relate  $u_i^G(\mathbf{x} - \mathbf{X})$  and  $\tau_{ij}^G(\mathbf{x} - \mathbf{X})$  to  $f_m$  by the relations

$$u_i^G = u_{i,m}^G f_m, \tag{2.2}$$

$$\tau_{ij}^G = \tau_{ij;m}^G f_m. \tag{2.3}$$

The solution for  $u_{i;m}^G$ , which is often called the Green's displacement tensor, is well known. It is

$$u_{i;m}^{G} = (\rho \omega^{2})^{-1} [-G_{L}(R) + G_{T}(R)]_{,im} + \mu^{-1} G_{T}(R) \delta_{im}$$
(2.4)

where

$$G_{\beta}(R) = (1/4\pi R) \exp(ik_{\beta}R) \quad (\beta = L, T); \tag{2.5}$$

$$R = |\mathbf{x} - \mathbf{X}|; \tag{2.6}$$

$$k_L = \omega/c_L, \qquad c_L^2 = (\lambda + 2\mu)/\rho;$$
 (2.7)

$$k_T = \omega/c_T, \qquad c_T^2 = \mu/\rho. \tag{2.8}$$

The corresponding expression for  $\tau_{ij;m}^G$  follows from Hooke's law, which is given by Eq. (1.1).

## 2.2. Integral representation for the displacement

Let V be a bounded domain and let S be its boundary surface. Let  $S_{\Gamma}$  be a sphere with radius  $\Gamma$  around a point of observation Q (outside V), and let  $V_{\Gamma}$  denote the domain interior to  $S_{\Gamma}$ , where  $\Gamma$  is chosen so large that  $S_{\Gamma}$  completely surrounds S. By using the elastodynamic reciprocity relation and the appropriate radiation condition, the displacement in  $V_{\infty}$ , where  $V_{\infty} = \lim_{\Gamma \to \infty} V_{\Gamma} - V$ , is expressed in terms of  $u_i$  and  $\tau_{ij}$  on S by the following integral representation, see e.g. [16],

$$u_m(\mathbf{x}) = -\int_{\mathbf{S}} \left[ \tau_{ij;m}^G(\mathbf{x} - \mathbf{X}) u_i(\mathbf{X}) - u_{i;m}^G(\mathbf{x} - \mathbf{X}) \tau_{ij}(\mathbf{X}) \right] n_j \, d\mathbf{A}(\mathbf{X})$$
(2.9)

where  $n_i$  is the outer normal, i.e. in this case  $n_i$  points into V.

Now consider an isolated flat crack of area A in an unbounded solid as shown in Fig. 1. The origin of the  $x_i$  coordinate system is near the crack. We also define a coordinate system  $\xi_i$ , whose origin O' is in the plane of

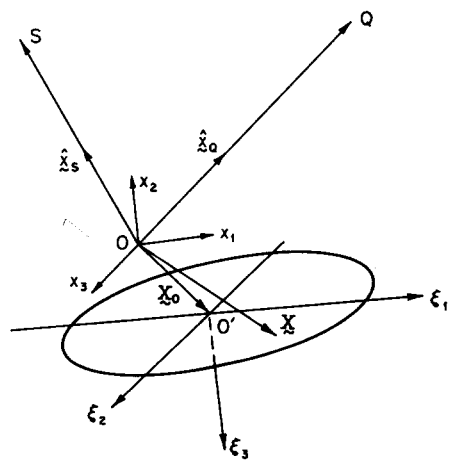


Fig. 1. Flat crack, with source point S and point of observation Q.

the crack, and whose  $\xi_3$ -axis is normal to that plane. Suppose the crack faces  $A^+(\xi_3 = 0^+)$  and  $A^-(\xi_3 = 0^-)$  are subjected to tractions  $t_i^+(X)$  and  $t_i^-(X)$ . If, as is typically the case, no net tractions act on the crack, we have  $\Delta t_i = t_i^+ - t_i^- = 0$ , which implies  $\Delta \tau_{ij} = 0$ . For a point in the body Eq. (2.9) then reduces to

$$u_m(\mathbf{x}) = \int_{\mathbf{A}^+} \tau_{ij;m}^G(\mathbf{x} - \mathbf{X}) \, \Delta u_i(\mathbf{X}) n_i^+ \, \mathrm{d}A(\mathbf{X}). \tag{2.10}$$

Here  $n_i^+$  is still an outer normal, and it is thus directed from the + to the - face of the crack.

Suppose a displacement wave  $u^{in}(x)$  is incident on the traction-free flat crack. The components of the stress tensor corresponding to the incident wave are  $\tau_{ij}^{in}(x)$ . The incident wave generates a scattered field  $u^{sc}(x)$ , such that the total displacement field is defined as

$$\boldsymbol{u}^{t}(\boldsymbol{x}) = \boldsymbol{u}^{in}(\boldsymbol{x}) + \boldsymbol{u}^{sc}(\boldsymbol{x}). \tag{2.11}$$

The scattered field does of course satisfy Eqs. (1.1)–(1.3), and consequently the representation (2.10) is valid for the scattered field.

# 2.3. Far-field integral representation

If terms of order O(|X|/|x|) are neglected, Eq. (2.4) yields the following expression for the far-field stresses

$$\tau_{ii:m}^{G} = ik_{I}b_{ii:m}^{G;L}(\hat{\boldsymbol{x}})G_{L}(x)\exp(-ik_{L}\hat{\boldsymbol{x}}\cdot\boldsymbol{X}) + ik_{T}b_{ii:m}^{G,T}(\hat{\boldsymbol{x}})G_{T}(x)\exp(-ik_{T}\hat{\boldsymbol{x}}\cdot\boldsymbol{X})$$
(2.12)

where  $\hat{x}$  is the unit vector in the direction of x, and x = |x|. Also

$$b_{ii:m}^{G;L}(\hat{x}) = (\lambda + 2\mu)^{-1} (2\mu \hat{x}_i \hat{x}_i + \lambda \delta_{ij}) \hat{x}_m, \tag{2.13}$$

$$b_{ij;m}^{G;T}(\hat{\mathbf{x}}) = \delta_{im}\hat{\mathbf{x}}_j + \delta_{jm}\hat{\mathbf{x}}_i - 2\hat{\mathbf{x}}_i\hat{\mathbf{x}}_j\hat{\mathbf{x}}_m. \tag{2.14}$$

It is easily checked that the longitudinal and transverse parts of the far field displacements have only components parallel and normal to x, respectively.

By virtue of Eq. (2.12) the representation integral for scattered far-field longitudinal motions now reduces to the form

$$[u_m^{\text{sc}}(\mathbf{x})]^L = -ik_L b_{ii:m}^{G;L}(\hat{\mathbf{x}}) G_L(\mathbf{x}) n_i I_i^L(\hat{\mathbf{x}})$$
(2.15)

where

$$I_{i}^{L}(\hat{\boldsymbol{x}}) = \int_{A^{+}} \exp(-\mathrm{i}k_{L}\hat{\boldsymbol{x}} \cdot \boldsymbol{X}) \,\Delta u_{i}^{\mathrm{sc}} \,\mathrm{d}A(\boldsymbol{X}). \tag{2.16}$$

#### 2.4. Physical elastodynamics

The simplest way to proceed from here is to employ an approximation analogous to the one of "physical optics". In this approximation, which we label the "physical elastodynamics" approximation, it is assumed that the displacement on the crack face in the shadow zone (i.e. at  $\xi_3 = 0^+$ ) is zero, and that on the illuminated crack face the total displacement u' is given by the total field associated with reflection of the incident wave from a traction-free plane surface. The latter is given by  $(u^{in} + u^{re})_{\xi_3 = 0^-}$ , where  $u^{re}$  represents the reflected displacement. Since  $u^t = u^{in} + u^{sc}$ , see Eq. (2.11), it follows that

$$\Delta u^{\text{sc}} = (u^{\text{t}} - u^{\text{in}})_{\xi_3 = 0^+} - (u^{\text{t}} - u^{\text{in}})_{\xi_3 = 0^-} = -(u^{\text{in}})_{\xi_3 = 0} - (u^{\text{in}} + u^{\text{re}} - u^{\text{in}})_{\xi_3 = 0^-}$$
(2.17)

or

$$\Delta u^{\rm sc} = -(u^{\rm in} + u^{\rm re})_{\xi_3 = 0^-}. \tag{2.18}$$

Let us consider a spherical wave emanating from the source point S shown in Fig. 1. The incident displacement wave may then be expressed in the form

$$\mathbf{u}^{\text{in}} = -(\mathbf{i}A/k_L)\nabla G_L(|\mathbf{x} - \mathbf{x}_S|) \tag{2.19}$$

where  $G_L(-)$  is defined by Eq. (2.5). For  $x_S \gg X$  we then have on the faces of the crack

$$\boldsymbol{u}^{\text{in}} \sim -A\hat{\boldsymbol{x}}_S G_L(\boldsymbol{x}_S) \exp(-\mathrm{i}k_L \hat{\boldsymbol{x}}_S \cdot \boldsymbol{X}). \tag{2.20}$$

As before we define  $x_s = |x_s|$  and X = |X|. Equation (2.20) represents a plane wave. The reflection of a plane wave from a traction-free surface is a simple problem whose solution can be found in textbooks, see e.g. [15]. On the reflecting surface  $\xi_3 = 0^-$  we may write

$$(\boldsymbol{u}^{\text{in}} + \boldsymbol{u}^{\text{re}})_{\xi_3 = 0^-} = -\boldsymbol{A}\boldsymbol{\alpha}(\hat{\boldsymbol{x}}_S)\boldsymbol{G}_L(\boldsymbol{x}_S) \exp(-\mathrm{i}\boldsymbol{k}_L\hat{\boldsymbol{x}}_S \cdot \boldsymbol{X}). \tag{2.21}$$

The vector  $\alpha(\hat{x}_S)$ , which depends on the direction (defined by  $x_S$ ) of the incident wave, is stated in the Appendix. Combining (2.21) and (2.18), and substituting the result in Eq. (2.15) yields

$$\frac{\left[u_{m}^{\text{sc}}(\mathbf{x}_{Q})\right]^{L}}{G_{L}(\mathbf{x}_{S})G_{L}(\mathbf{x}_{Q})} = -A\alpha_{i}(\hat{\mathbf{x}}_{S})b_{ij;m}^{G;L}(\hat{\mathbf{x}}_{Q})n_{i}I(k_{L})$$
(2.22)

where

$$I(k_L) = ik_L \int_{\mathbf{A}^+} \exp(-ik_L \mathbf{q} \cdot \mathbf{X}) \, d\mathbf{A}(\mathbf{X})$$
(2.23)

and

$$q = \hat{\mathbf{x}}_Q + \hat{\mathbf{x}}_S. \tag{2.24}$$

It is convenient to express the area integral given by Eq. (2.23) in terms of the  $\xi_i$  coordinate system whose origin O' is located in the plane of the crack as shown in Fig. 1. Writing

$$X = X_O + \xi;$$
  $q = \hat{x}_O + \hat{x}_S = (X_O + \xi_O)/x_O + (X_O + \xi_S)/x_S$  (2.25a,b)

we find

$$I(k_L) = ik_L \exp(-ik_L \chi) \iint_{A^+} \exp(-ik_L \mathbf{q} \cdot \boldsymbol{\xi}) \, d\xi_1 \, d\xi_2$$
 (2.25)

where

$$\chi = (\hat{\mathbf{x}}_Q + \hat{\mathbf{x}}_S) \cdot \mathbf{X}_O \tag{2.26}$$

It should be noted that in the general inverse problem the position of O is selected and thus  $\hat{x}_O + \hat{x}_S$  is known. The plane of the crack is, however, generally unknown, hence  $X_O$  is unknown. The area integral in Eq. (2.25) can be reduced to a line integral over the crack edge C by noting that  $I(k_L)$  can also be expressed in the form

$$I(k_L) = -\frac{\exp(-ik_L\chi)}{q_1^2 + q_2^2} \iint_{A^+} \frac{\partial}{\partial \xi_i} [q_i \exp(-ik_L \boldsymbol{q} \cdot \boldsymbol{\xi})] d\xi_1 d\xi_2; \quad i = 1, 2$$
(2.27)

where  $q_1$  and  $q_2$  are the components of  $\mathbf{q}$  in the  $\xi_i$ -system. An application of the divergence theorem subsequently yields

$$I(k_L) = -\frac{\exp(-ik_L \chi)}{q_1^2 + q_2^2} \int_C \nu_i q_i \exp(-ik_L \mathbf{q} \cdot \mathbf{\xi}) ds$$
 (2.28)

where  $v_i$  (i = 1, 2) is the outward unit normal to the crack edge, and s is arc length measured along the crack edge. By means of Eqs. (2.28) and (2.22) the scattered longitudinal field is expressed as radiation generated by a superposition of sources over the edge of the crack. This kind of representation seems to be analogous to the method of equivalent currents, which has been explored by several authors in electromagnetic scattering, see eg. Knott and Senior [17].

A convenient alternate form of Eq. (2.28) is obtained by introducing a new set of coordinates  $(\bar{\xi}_1, \bar{\xi}_2)$  in the plane of the crack. The  $\bar{\xi}_1$  coordinate is taken along the projection of  $\boldsymbol{q}$  on the plane of the crack, see Fig. 2. The coordinate transformation is given by

$$\bar{\xi}_1 = q_1 \xi_1 + q_2 \xi_2, \tag{2.29}$$

$$\bar{\xi}_2 = -q_2 \xi_1 + q_1 \xi_2.$$
 (2.30)

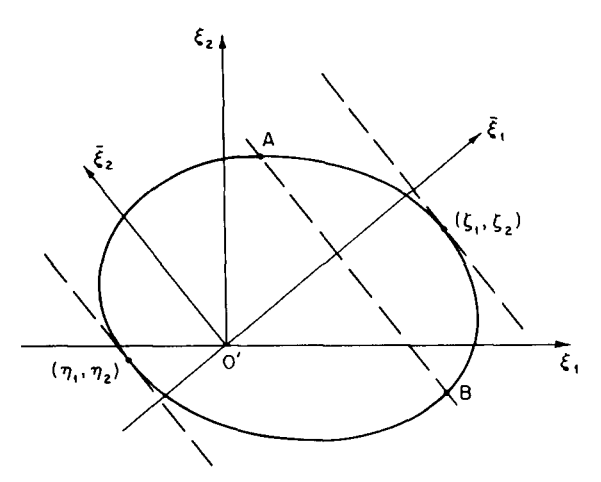


Fig. 2. Coordinates in the plane of the crack.

It is easily checked that Eq. (2.28) can then be rewritten as

$$I(k_L) = -\frac{\exp(-ik_L\chi)}{a_1^2 + a_2^2} \int_C \exp(-ik_L\bar{\xi}_1) d\bar{\xi}_2.$$
 (2.31)

A useful approximation to the integral in Eq. (2.31) can be derived by making use of a system of local coordinates for the curve C. Let the two tangents parallel to  $\bar{\xi}_1$  = constant touch the edge C at the points  $(\xi_1, \xi_2)$  and  $(\eta_1, \eta_2)$  defined in the  $(\bar{\xi}_1, \bar{\xi}_2)$  system in the plane of the crack. Near  $(\xi_1, \xi_2)$  the points of C can be expressed approximately by

$$\bar{\xi}_1 = \zeta_1 + \frac{1}{2!} s^2 \beta_0 + \frac{1}{3!} s^3 \beta_1, \tag{2.32}$$

$$\bar{\xi}_2 = \zeta_2 + s - \frac{1}{3!} s^3 \beta_0^2 \tag{2.33}$$

where  $\beta_0$  and  $\beta_1$  denote the curvature of C and its derivative w.r.t s at  $(\zeta_1, \zeta_2)$  and s is the arc length measured from this point, which can be positive or negative. Substituting Eqs. (2.32) and (2.33) into Eq. (2.31) and retaining terms of  $O(s^2)$  only, the contribution to  $I(k_L)$  from the neighborhood of  $(\zeta_1, \zeta_2)$  is obtained as

$$I(k_L) \approx -\frac{\exp(-ik_L(\chi + \zeta_1))}{a_1^2 + a_2^2} \int_{|s| \le 1} \exp(-ik_L s^2 \beta_0 / 2!) ds \approx -\frac{(2\pi)^{1/2} e^{-i\pi/4}}{(a_1^2 + a_2^2)(\beta_0)^{1/2}} \frac{\exp(-ik_L(\chi + \zeta_1))}{k_L^{1/2}}$$
(2.34)

where the stationary phase approximation, which is valid for high frequencies, has been used. When combined with (2.22) the above approximation confirms the familiar  $(1/k_L^{1/2})$  behavior predicted by geometrical diffraction theory. A similar conclusion holds good for the contribution from the neighborhood of the other point  $(\eta_1, \eta_2)$  whose tangent is also parallel to  $\bar{\xi}_1$  = constant.

## 3. Inversion integrals

We will now turn our attention to the inverse problem, i.e., to the problems of determining size, shape and orientation of a crack from the scattered field.

The general forms of Eqs. (2.28), (2.31) and (2.34) suggest a formal application of an exponential Fourier-type integral, with  $k_L$  as the variable, to both sides of Eq. (2.22). We will consider two inversion integrals:

$$f_1^* = \mathcal{J}_1\{f(k_L)\} = \int_{-\infty}^{\infty} \exp(\mathrm{i}k_L \mathbf{q} \cdot \mathbf{\lambda}) f(k_L) \, \mathrm{d}k_L, \tag{3.1}$$

$$f_2^* = \mathcal{J}_2\{f(k_L)\} = \int_{-\infty}^{\infty} k_L^{1/2} \exp(\mathrm{i}k_L \mathbf{q} \cdot \mathbf{\lambda}) f(k_L) \, \mathrm{d}k_L. \tag{3.2}$$

Both inversion integrals will be evaluated by using the following general property

$$\int_{-\infty}^{\infty} \exp(ik_L(\boldsymbol{q} \cdot \boldsymbol{\lambda} - \gamma)) dk_L = 2\pi\delta(\boldsymbol{q} \cdot \boldsymbol{\lambda} - \gamma). \tag{3.3}$$

In Eqs. (3.1)–(3.3) the vector  $\lambda$  defines a test point in the body, defined either in the  $x_i$  or the  $\xi_i$  coordinate system. The vector  $\mathbf{q}$  is either  $\mathbf{q} = \hat{\mathbf{x}}_Q + \hat{\mathbf{x}}_S$  or  $\mathbf{q} = (\mathbf{X}_Q + \boldsymbol{\xi}_Q)/x_Q + (\mathbf{X}_Q + \boldsymbol{\xi}_S)/x_S$ , depending on which coordinate system is operational.

For two special cases the inversion integrals given by (3.1) and (3.2) yield explicit information on the crack in a simple manner from the scattered field at a limited number of points. These special cases are that either the plane of the crack is known a-priori or that a plane of symmetry of the crack is known. In both cases it must also be assumed that an origin of the  $\mathcal{E}_i$ -system can be selected in the vicinity of the crack.

## 3.1. Plane of the crack is known a-priori

If the plane in which the crack is located is known a-priori, the  $x_i$  coordinate system can be taken to coincide with the  $\xi_i$  system. Thus we have  $X_0 = 0$ , and Eq. (2.22) becomes

$$\frac{\left[u_m^{\text{sc}}(\boldsymbol{\xi}_Q)\right]^L}{G_I(\boldsymbol{\xi}_S)G_I(\boldsymbol{\xi}_Q)} = A\alpha_i(\hat{\boldsymbol{\xi}}_S)b_{i3;m}^{G;L}(\boldsymbol{\xi}_Q)I(k_L)$$
(3.4)

where it has been taken into account that in the  $\xi_i$ -system  $n_i^+$  is a unit vector in the  $-\xi_3$  direction. The integral  $I(k_L)$  is defined by one of the forms (2.28), (2.31) or (2.34) and

$$q = \hat{\boldsymbol{\xi}}_{Q} + \hat{\boldsymbol{\xi}}_{S}. \tag{3.5}$$

For this special case we will apply both the inversion integrals  $\mathcal{I}_1$  and  $\mathcal{I}_2$ , which are defined by Eqs. (3.1) and (3.2), respectively.

The formal operation defined by Eq. (3.1) can conveniently be applied to the line integral given by Eq. (2.31). After an interchange of the order of integration and employing Eq. (3.3) we obtain

$$I_1^* = -\frac{2\pi}{q_1^2 + q_2^2} \int_C \delta(\mathbf{q} \cdot \mathbf{\lambda} - \bar{\xi}_1) \, d\bar{\xi}_2. \tag{3.6}$$

On the crack edge C,  $\bar{\xi}_1$  is a function of  $\bar{\xi}_2$ , which suggests a change of integration variable to yield

$$I_1^* = -\frac{2\pi}{q_1^2 + q_2^2} \int_C \delta(\boldsymbol{q} \cdot \boldsymbol{\lambda} - \bar{\xi}_1) \left(\frac{\mathrm{d}\bar{\xi}_2}{\mathrm{d}\bar{\xi}_1}\right) \mathrm{d}\bar{\xi}_1. \tag{3.7}$$

Now we select  $\lambda$  in the plane of the crack. Then,  $q \cdot \lambda$  defines the component  $\bar{\lambda}_1$  in the  $\bar{\xi}_1$  direction, see Eq. (2.29). The relation  $q \cdot \lambda = \text{constant}$ , say  $q \cdot \lambda = \zeta$  defines a line normal to the  $\bar{\xi}_1$  axis. When this line intersects the crack edge C the delta-function in Eq. (3.7) becomes operative, and it sifts out the values of  $d\bar{\xi}_2/d\bar{\xi}_1$  at  $\bar{\xi}_1 = \zeta$ . We obtain

$$I_1^* = -\frac{2\pi}{q_1^2 + q_2^2} \left[ \left( \frac{d\bar{\xi}_2}{d\bar{\xi}_1} \right)^A + \left( \frac{d\bar{\xi}_2}{d\bar{\xi}_1} \right)^B \right]$$
 (3.8)

where the points A and B are defined in Fig. 2. When  $\eta_1 < q \cdot \lambda < \zeta_1$ , the integral given by Eq. (3.8) is bounded. Clearly when  $q \cdot \lambda < \eta_1$  or  $q \cdot \lambda > \zeta_1$  the integral is identically zero. For a smooth crack edge the integral becomes singular when either  $q \cdot \lambda = \eta_1$  or  $q \cdot \lambda = \zeta_1$ , with a singularity of square root order (see, for example, the discussion of an elliptical crack in the next section).

Next we investigate the application of the formal operator  $\mathcal{I}_2$ , defined by Eq. (3.2). This operator is most conveniently applied to the stationary phase approximation of the line integral, which is given by Eq. (2.34). The result is

$$I_2^* \approx -\frac{(2\pi)^{3/2}}{\beta_0^{1/2}} \frac{e^{-i\pi/4}}{q_1^2 + q_2^2} \delta(\boldsymbol{q} \cdot \boldsymbol{\lambda} - \zeta_1). \tag{3.9}$$

As before we take  $\lambda$  in the plane of the crack, which implies that  $q \cdot \lambda$  defines the component  $\tilde{\lambda_1}$  of  $\lambda$  in the  $\bar{\xi_1}$  direction. Equation (3.9) then shows that  $I_2^*$  displays a  $\delta$ -function behavior when  $\bar{\lambda_1} = \zeta_1$ . The same conclusion holds for  $\bar{\lambda_1} = \eta_1$ . Thus, application of  $\mathcal{I}_2$  to (2.34) yields an identically vanishing result when  $\bar{\lambda_1}$  is not equal to either  $\zeta_1$  or  $\eta_1$ .

The results of this section may now be summarized as follows. Equation (3.4) is a high frequency representation of the scattered longitudinal far-field. In this equation  $u_m^{sc}(\xi_Q)$  may be considered as known, say from experiments. Then, if we select a test point  $\lambda$  in the plane of the crack (which is known), then either the application of the operator  $\mathcal{I}_1$  or the operator  $\mathcal{I}_2$  to the right hand side of (3.4) yields a singularity at two values of  $q \cdot \lambda = \bar{\lambda}_1$ . These are  $\bar{\lambda}_1 = \zeta_1$  and  $\bar{\lambda}_1 = \eta_1$ . For  $\mathcal{I}_1$  the singularity is of the square root type, while for  $\mathcal{I}_2$  the singularity is a Dirac delta function. Equation (3.4) then implies that the application of these operators to the left-hand side of Eq. (3.4), i.e., to  $u_m^{sc}(\xi_Q)/G_L(\xi_S)G_L(\xi_Q)$ , where  $u_m^{sc}(\xi_Q)$  represent experimental data at the point of observation  $\xi_Q$ , should also produce singular behavior at two lines in the  $\xi_1\xi_2$ -plane. These lines define a strip  $\eta_1 < \bar{\lambda}_1 < \zeta_1$  containing the crack. By taking several points of

observation, i.e., several vectors  $\mathbf{q}$ , we can then construct an envelope of the crack edge. For a crack with a smooth edge four such strips should give a quite acceptable estimate of the crack size.

It would seem that a delta function has a more characteristic signature, and hence the operator  $\mathcal{I}_2$  may be preferable from the practical point of view.

# 3.2. Source and receiver are located in a known plane of symmetry of the crack

The geometry for this case is shown in Fig. 3. The position of the origin O of the coordinate system  $x_i$  is arbitrary, but O must be chosen close to the crack. The scattered field is given by Eq. (2.22). By using (2.25) and (2.34) we find

$$I(k_L) = -\frac{1}{q_1^2 + q_2^2} \left(\frac{2\pi}{k_L}\right)^{1/2} J \tag{3.10}$$

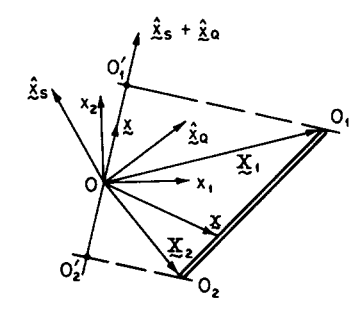


Fig. 3. Source and receiver in plane of symmetry of the crack.

where

$$J = \sum_{j=1}^{2} D_j \exp(-ik_L(\hat{\mathbf{x}}_Q + \hat{\mathbf{x}}_S) \cdot \mathbf{X}_j)$$
(3.11)

$$D_1 = \frac{1}{(\beta_0^{1/2})_1} e^{-i\pi/4}, \qquad D_2 = \frac{1}{(\beta_0^{1/2})_2} e^{i\pi/4}. \tag{3.12}$$

It is of interest to examine the absolute magnitude of J:

$$|J| = \{|D_1|^2 + |D_2|^2 + 2|D_1||D_2|\sin[k_L(\hat{x}_Q + \hat{x}_S) \cdot c]\}^{1/2}$$
(3.13)

where c is the "crack vector", which is defined as

$$\boldsymbol{c} = \boldsymbol{X}_1 - \boldsymbol{X}_2. \tag{3.14}$$

Equation (3.13) implies that the amplitude of the primary diffracted field is modulated with respect to  $k_L = \omega/c_L$  with period

$$P = \frac{2\pi}{(\mathbf{x}_Q + \mathbf{x}_S) \cdot \mathbf{c}}.\tag{3.15}$$

Experimental results for the amplitude spectrum, see e.g. Ref. [18], do indeed show this periodicity. Thus, if  $[u_m^{sc}(x_Q)]^L$  on the left-hand side of Eq. (2.22) represents experimental data, we can define  $P_Q$  as the period of  $[[u_m^{sc}(x_Q)]^L]$ . By virtue of Eq. (3.15) we then obtain

$$(\mathbf{x}_Q + \mathbf{x}_S) \cdot \mathbf{c} = 2\pi/P_Q. \tag{3.16}$$

Consequently from the observation at one location Q we obtain one strip normal to the bisector of  $\overline{OQ}$  and  $\overline{OS}$ , and of width  $2\pi/P_Q$ , which contains  $\Sigma$  where  $\Sigma$  is the trace of the crack in the plane of symmetry. For backscattering we take S as the second point of observation, to obtain

$$\mathbf{x}_{S} \cdot \mathbf{c} = \pi / P_{S} \tag{3.17}$$

where  $P_S$  is the period of  $|[u_m^{\text{sc}}(x_S)]^L|$ . Equation (3.17) defines a second strip, whose intersection with the first strip then leads us to four points of interaction out of which two alternate well defined possibilities for  $\Sigma$  emerge. The final determination of  $\Sigma$  is obtained by making use of data from just one more point of observation leading to a third strip whose intersections with the first two defines the vector c, i.e., the cross section of the crack with the normal plane containing source and observer.

The same conclusions are reached if the operator  $\mathcal{I}_2$  is applied to Eq. (3.10).

## 4. Application of the inversion technique to analytic and experimental examples

We now examine the application of the inversion technique to some analytical and experimental examples.

The first analytical example we consider is that of a crack of an elliptical shape for which a direct solution is known.

## 4.1. Crack of elliptical shape

For an elliptical crack of major axis a minor axis b the line integral over the edge C given by Eq. (2.28) can be evaluated explicitly. The simple expression that is obtained can be used to check the manipulations in the corresponding inverse problem.

Assuming that the origin is taken in the plane of the crack, we have  $X_0 \equiv 0$  and therefore  $\chi = 0$ .

To evaluate Eq. (2.28) we introduce new variables  $\varphi$  and  $\psi$  by the relations

$$(\xi_1, \xi_2) = [a\cos(\varphi + \psi), b\sin(\varphi + \psi)], \qquad 0 \le \varphi \le 2\pi, \tag{4.1}$$

$$(\cos \psi, \sin \psi) = \rho^{-1}(aq_1, bq_2),$$
 (4.2)

$$\rho = (a^2 q_1^2 + b^2 q_2^2)^{1/2}. (4.3)$$

It then follows that

$$(\nu_1, \nu_2) ds = [b \cos(\varphi + \psi), a \sin(\varphi + \psi)] d\varphi$$
(4.4)

and Eq. (2.28) becomes

$$I(k_L) = -\frac{\rho}{q_1^2 + q_2^2} \int_0^{2\pi} \left[ \frac{b}{a} \cos(\varphi + \psi) \cos \psi + \frac{a}{b} \sin(\varphi + \psi) \sin \psi \right] \exp(-ik_L \rho \cos \varphi) d\varphi. \tag{4.5}$$

This integral can be further evaluated to yield

$$I(k_L) = -(2\pi i ab/\rho)J_1(k_L\rho)$$
 (4.6)

where  $J_1($  ) is the ordinary Bessel function of order one, and  $\rho$  is defined by Eq. (4.3). Upon substitution of (4.6) into Eq. (2.22) we obtain the scattered longitudinal field associated with physical elastodynamics for an elliptical crack.

We now apply the inverse procedure to the above solution starting with  $I(k_L)$  as given by Eq. (4.6), and recover the elliptical shape as a check on our method. The inverse operator Eq. (3.1) when applied to Eq. (4.6) yields

$$I_1^* = -\frac{2\pi i ab}{\rho} \int_{-\infty}^{\infty} \exp(ik_L \boldsymbol{q} \cdot \boldsymbol{\lambda}) J_1(k_L \rho) \, dk_L = \frac{2\pi ab}{\rho} \int_{0}^{\infty} \sin(k_L \boldsymbol{q} \cdot \boldsymbol{\lambda}) J_1(k_L \rho) \, dk_L. \tag{4.7}$$

This is a known integral which has the value

$$I_{1}^{*} = \begin{cases} \frac{2\pi ab}{\rho^{2}} \frac{\boldsymbol{q} \cdot \boldsymbol{\lambda}}{[\rho^{2} - (\boldsymbol{q} \cdot \boldsymbol{\lambda})^{2}]^{1/2}} & \text{if } 0 < |\boldsymbol{q} \cdot \boldsymbol{\lambda}| < \rho, \\ 0 & \text{if } |\boldsymbol{q} \cdot \boldsymbol{\lambda}| > \rho. \end{cases}$$

$$(4.8)$$

For a variable test point  $\lambda$  in the plane of the crack, we thus get square root singularities on the lines

$$q \cdot \lambda = \pm \rho \tag{4.9}$$

Specifically, if

$$\lambda = (x_1, x_2, 0) \tag{4.10}$$

these lines are given by

$$q_1x_1 + q_2x_2 = \pm (a^2q_1^2 + b^2q_2^2)^{1/2}. (4.11)$$

It is easily verified that Eq. (4.11) describes a pair of tangents to the ellipse

$$x_1^2/a^2 + x_2^2/b^2 = 1 (4.12)$$

with the points of contact at

$$\left(\pm \frac{q_1 a^2}{(a^2 q_1^2 + b^2 q_2^2)^{1/2}}, \pm \frac{q_2 b^2}{(a^2 q_1^2 + b^2 q_2^2)^{1/2}}\right). \tag{4.13}$$

Thus, taking different positions for the observation points Q, we can construct the boundary of the elliptical crack as the envelope of the various tangents given by Eq. (4.11).

A similar conclusion will follow if we employ the inverse operator Eq. (3.2) to Eq. (4.6). It appears, however, that in this case we will get  $\delta$ -function singularities at the same positions as in Eq. (4.11) only if we employ the asymptotic expression for the Bessel function at large  $k_L \rho$ .

# 4.2. Numerical examples

We now consider some computational aspects of interest for both the analytical and the experimental examples. Our discussion will be mainly for the two-dimensional cracks or for cases when the source and receiver are in a plane of symmetry of the crack. These considerations will however be equally useful for the 3-D cases.

From high-frequency diffraction theories, the far-field can be expressed as essentially a sum of two flash-point contributions from which the expression  $I(k_L)$  such as that given by Eqs. (3.10) and (3.11) arise.

The expression in Eq. (3.11) is, however, only an approximation to the more general form

$$J = \sum_{j=1}^{2} D_{j} \exp(ik_{L}(\overline{SO_{j}} + \overline{O_{j}Q} - \overline{SO} - \overline{OQ}))$$
(4.14)

which involves the actual values of the ray paths through each of the flash points or in 2-D, the crack tips  $O_i$ , and accounts for the factor  $G_L(x_S)G_L(x_O)$  by which we divide  $\left[u_m^{\rm sc}(x_O)\right]^L$  as in Eq. (2.22).

While applying the inverse operator as in Eq. (3.1) or Eq. (3.2) it is recalled that the resulting planes across which the singularities appear will depend on the exponents in Eq. (3.11) or equivalently, those in Eq. (4.14). The exponents in these two cases will be slightly different in their respective values, the effect of which will now be studied. The inverse operator in Eq. (3.1) when applied to the two terms in Eq. (3.11) will yield  $\delta$ -function singularities along the lines

$$(\hat{\mathbf{x}}_O + \hat{\mathbf{x}}_S) \cdot (\boldsymbol{\lambda} - \boldsymbol{X}_i) = 0 \quad (i = 1, 2). \tag{4.15}$$

Equation (4.15) defines a strip on whose boundaries the tips of the crack are located. Similarly, from an observation of the backscatter at S, we get another strip defined by

$$\hat{\boldsymbol{x}}_{S} \cdot (\boldsymbol{\lambda} - \boldsymbol{X}_{i}) = 0 \quad (j = 1, 2). \tag{4.16}$$

The locations of the crack tips can then be found from the intersections of the strips in Eq. (4.15) and Eq. (4.16). The final choice between the two emerging alternatives will then be decided by constructing a strip from just one more observation point.

In practice, however, the exponents in Eq. (4.14) which we will actually use for the inversion, lead to slightly modified strips. The points of intersections may then shift by amounts not necessarily small in comparison with crack lengths. To rectify such errors we use an iterative scheme described below.

#### 4.3. The iterative scheme

The inverse operator Eq. (3.1) when applied to Eq. (4.14) yields the strip

$$(\hat{\mathbf{x}}_S + \hat{\mathbf{x}}_O) \cdot \mathbf{\lambda} = -(\overline{SO}_i + \overline{O_iQ} - \overline{SO} - \overline{OQ}) \tag{4.17}$$

from the observation at Q, and similarly the strip

$$\hat{\mathbf{x}}_{S} \cdot \mathbf{\lambda} = -(\overline{SO}_{i} - \overline{SO}) \tag{4.18}$$

from the backscatter at S.

Let the approximate crack tips determined by these strips be denoted by  $X_i^{(0)}$ . Replace  $\lambda$  by  $X_i^{(0)}$  in Eqs. (4.17) and (4.18) and rewrite these equations in the form

$$(\hat{\boldsymbol{x}}_S + \hat{\boldsymbol{x}}_Q) \cdot (\boldsymbol{X}_i - \boldsymbol{X}_i^{(0)}) = \varepsilon_i^S + \varepsilon_i^Q, \tag{4.19}$$

$$\hat{\boldsymbol{x}}_{S} \cdot (\boldsymbol{X}_{i} - \boldsymbol{X}_{i}^{(0)}) = \varepsilon_{i}^{S}, \tag{4.20}$$

where

$$\varepsilon_{j}^{S} = SO_{j} - SO + \hat{\mathbf{x}}_{S} \cdot \mathbf{X}_{j}, \tag{4.21}$$

$$\varepsilon_j^Q = O_j Q - OQ + \hat{\boldsymbol{x}}_Q \cdot \boldsymbol{X}_j. \tag{4.22}$$

Equations (4.19) and (4.20) can now be solved by an iterative scheme for the crack-tip positions  $X_i$  by taking  $X_i^{(0)}$  as the first approximation. We then evaluate  $\varepsilon_i^S$  and  $\varepsilon_i^Q$  at  $X_i^{(0)}$  and substitute in Eqs. (4.19) and (4.20) to solve for the next higher order value of  $X_i$ , and repeat this cycle till necessary. We find that four to five iterations are usually adequate. Some numerical results are discussed below.

### 4.4. Results for the analytic examples

For our numerical calculations we consider the case of a crack shown in Fig. 4. The crack half-length is taken as the unit of length. The angles  $\theta_1$ ,  $\theta_2$ ,  $\theta_3$ ,  $\theta_4$  and the distances  $\overline{OS}$ ,  $\overline{OQ}$  and  $\overline{OC}$ , where C is the center of the crack, form the various parameters. The computed results giving the errors in the crack-edge calculations are shown in Figs. 5, 6 and 7 which also include the effect of iterative corrections along with results without any iterations. The edge-error is the absolute distance between the actual and computed positions of the edge concerned.

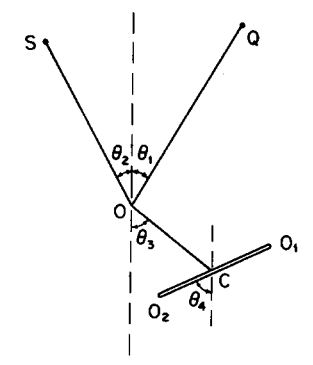


Fig. 4. Geometry for numerical calculations.

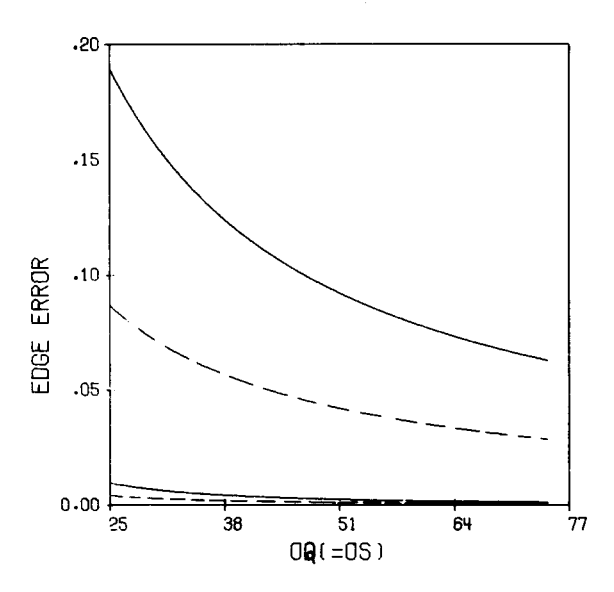


Fig. 5. Edge error for edge  $O_1$  versus OQ (=OS);  $\theta_1 = 0.523$ ,  $\theta_2 = 0.698$ ,  $\theta_3 = 0.698$ ,  $\theta_4 = 0.785$  (radians):— $\overline{OC} = 3$ ,  $---\overline{OC} = 2$ . No iteration for upper curves; one iteration for lower curves.

#### 4.5. Experimental results

As mentioned earlier, the inversion technique was applied also to the case of experimentally measured far-field results in a plane of symmetry of the crack reported in Ref. [18]. The model shown in Fig. 8 is that of a penny-shaped crack of radius  $2500 \,\mu$  centrally located in a titanium block of height  $2.5 \,\mathrm{cm}$  and

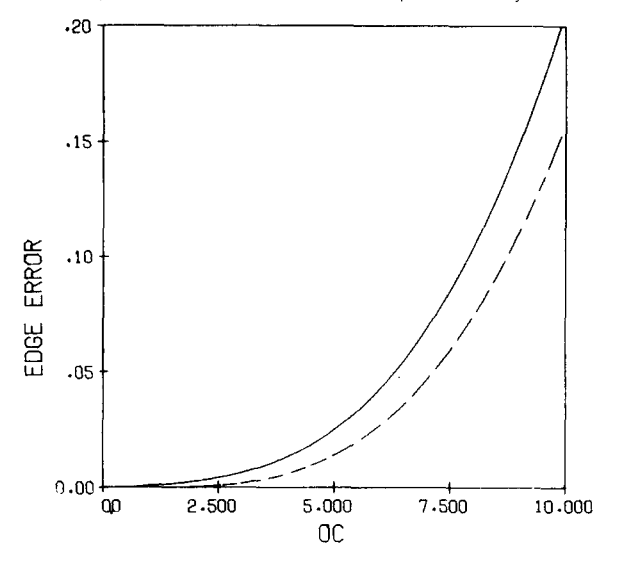


Fig. 6. Edge error for edges  $O_1$  (----) and  $O_2$  (----) versus  $\overline{OC}$ ;  $\theta_1 = 0.523$ ,  $\theta_2 = 0.698$ ,  $\theta_3 = 0.698$ ,  $\theta_4 = 0.785$  (radians).  $\overline{OQ} = \overline{OS} = 30$ . Number of iterations = 10.

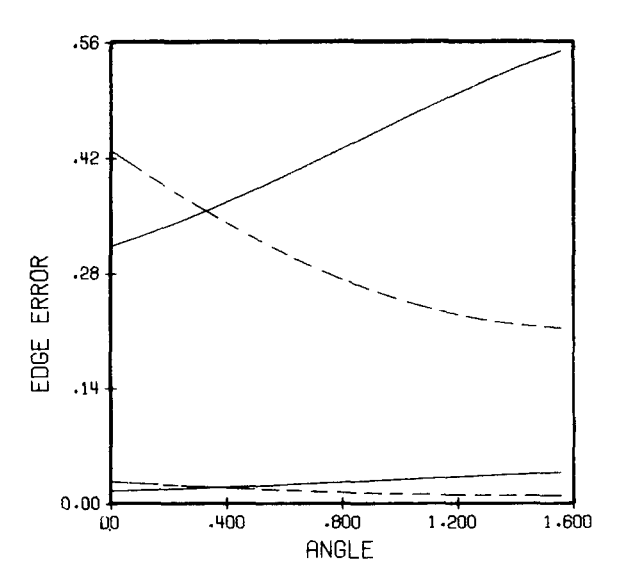


Fig. 7. Edge error for edges  $O_1$  (——) and  $O_2$  (----) versus angle  $\theta_4$ ,  $\theta_1 = 0.523$ ,  $\theta_2 = 0.698$ ,  $\theta_3 = 0.698$  (radians).  $\overline{OC} = 5$ ,  $\overline{OQ} = \overline{OS} = 30$ . No iteration for upper curves; one iteration for lower curves.

cross-width of 10 cm. The block was immersed in water, and it was excited by a source on the axis of symmetry, far out in the water. The scattered field was measured at a number of points in the water, and the measurements were then referred to points on the interface. The period of amplitude-modulation at these points are measured and given in Table 1 using the notation of Figure 8.

For the additional information to complete the far-field we assumed that the location of the crack center is given. We then used the iterative scheme to predict the crack-orientation angle as well as its radius. The

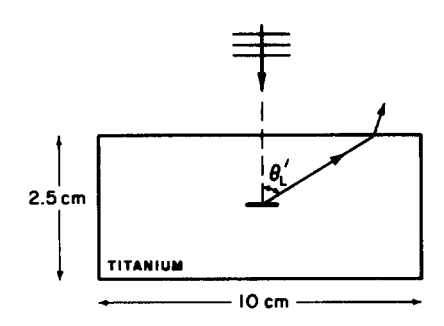


Fig. 8. Sketch of experimental configuration in Ref. [18].

Table 1 Period of amplitude modulations for several angles  $\theta_L^\prime$ 

Scattering angle	Period of average	
$(\theta_L')$	amplitude modulation	
	$(\Delta f)_{ave}$ (in MHz)	
35°	2.18	
40°	1.87	
45°	1.83	
50°	1.68	
55°	1.60	
60°	1.47	
65°	1.39	

results which are summarized in Table 2 generally indicate better estimates from widely separated points of observation.

# 4.6. Comments on band-limited observations

From the practical standpoint there is a limit on the bandwidths where one can record the observations. In our inverse operator  $\mathcal{I}_2$  in Eq. (3.2), this amounts to restricting  $k_L$  to

$$k_{-} < |k_{L}| < k_{+}$$
 (4.23)

Table 2
Results of inversion procedure for several pairs of scattering angles

Angles	(degrees)	Radius	Crack angle
65.0	35.0	2497.9	89.73
65.0	40.0	2357.4	87.50
65.0	45.0	2641.3	-88.29
65.0	50.0	2663.1	-88.01
65.0	55.0	2965.8	-84.62
65.0	60.0	2775.0	-86.66
35.0	40.0	3307.1	-85.83
35.0	45.0	2180.3	87.03
35.0	50.0	2313.9	88.26
35.0	55.0	2241.6	87.62
35.0	60.0	2436.0	89.26

where  $k_-$  and  $k_+$  are fixed. For an ideal inversion the operator  $\mathcal{I}_2$  must produce a pair of delta functions to define a strip (or layer). We need to establish some criteria on the choice of  $k_-$  and  $k_+$  to ensure recognizable  $\delta$ -type behavior.

For this purpose consider the integral representation of the delta function

$$2\pi\delta(x) = \int_{-\infty}^{\infty} \exp(\mathrm{i}k_L x) \, \mathrm{d}k_L = 2 \int_{0}^{\infty} \cos(k_L x) \, \mathrm{d}k_L. \tag{4.24}$$

Corresponding to the assumption in Eq. (4.23) let the approximation to  $\delta(x)$  be

$$\delta(x) = (1/\pi)\Delta(x) \tag{4.25}$$

where

$$\Delta(x) = \int_{k_{-}}^{k_{+}} \cos(k_{L}x) \, \mathrm{d}k_{L} = \frac{\sin(k_{L}x)}{x} \bigg|_{k_{-}}^{k_{+}}. \tag{4.26}$$

The function  $\Delta(x)$  has been computed as a function of x (for x > 0) and shown in Fig. 9 for different combinations of  $k_+$  and  $k_-$ . The four cases (A) to (D) there correspond to  $k_+ = 2$ , 6, 10 and 14 with  $k_- = 1$  for all the cases. The peak at x = 0 is conspicuous for all the cases with  $k_+ \ge 6$ . The case when  $k_+ = 2$  indicates too small a bandwidth and, therefore, the peak at x = 0 is not very strong.

# Appendix. Computation of the COD factor $\alpha_i(\phi_L)$

The COD-factor  $\alpha_i(\phi_L)$  is computed by considering the reflection of a plane longitudinal wave defined by

$$\boldsymbol{u}^{L} = A\boldsymbol{p}^{L} \exp(\mathrm{i}k_{L}\boldsymbol{p}^{L} \cdot \boldsymbol{\xi}) \tag{A.1}$$

from the free surface defined by  $\xi_3 = 0$ . The propagation vector of the incident wave is defined by

$$\mathbf{p}^{L} = (\sin \phi_{L} \cos \theta, \sin \phi_{L} \sin \theta, \cos \phi_{L}). \tag{A.2}$$

Expressions for the reflected waves can be found in textbooks, see e.g. Ref. [15], p. 42. The total displacement field, which comprises the incident longitudinal wave and the reflected longitudinal and transverse waves is given by

$$\boldsymbol{u}^{t} = \boldsymbol{A}[\boldsymbol{p}^{L} \exp(\mathrm{i}k_{L}\boldsymbol{p}^{L} \cdot \boldsymbol{\xi}) + \boldsymbol{R}_{L}^{L}(\phi_{L})\boldsymbol{p}^{Lr} \exp(\mathrm{i}k_{L}\boldsymbol{p}^{Lr} \cdot \boldsymbol{\xi}) + \boldsymbol{R}_{T}^{L}(\phi_{L})\boldsymbol{d}^{\mathrm{Tr}} \exp(\mathrm{i}k_{T}\boldsymbol{p}^{\mathrm{Tr}} \cdot \boldsymbol{\xi})]$$
(A.3)

where the propagation vectors of the reflected waves are given by

$$\mathbf{p}^{\alpha r} = (\sin \phi_{\alpha} \cos \theta, \sin \phi_{\alpha} \sin \theta, -\cos \phi_{\alpha}) \tag{A.4}$$

where  $\alpha = L$  and  $\alpha = T$ , and the angles  $\phi_L$  and  $\phi_T$  are related by Snell's law

$$\sin \phi_T = \chi^{-1} \sin \phi_L; \qquad \chi = c_L/c_T. \tag{A.5}$$

The direction of the displacement corresponding to the reflected wave of transverse motion is defined by

$$\boldsymbol{d}^{\mathrm{Tr}} = (\cos \phi_T \cos \theta, \cos \phi_T \sin \theta, \sin \phi_T) \tag{A.6}$$

and the reflection coefficients are

$$R_L^L(\phi_L) = D^{-1}(\sin 2\phi_L \sin 2\phi_T - \kappa^2 \cos^2 2\phi_T),$$
 (A.7)

$$R_T^L(\phi_L) = D^{-1}(2\kappa \sin 2\phi_L \cos 2\phi_T), \tag{A.8}$$

$$D = \sin 2\phi_L \sin 2\phi_T + \kappa^2 \cos^2 2\phi_T. \tag{A.9}$$

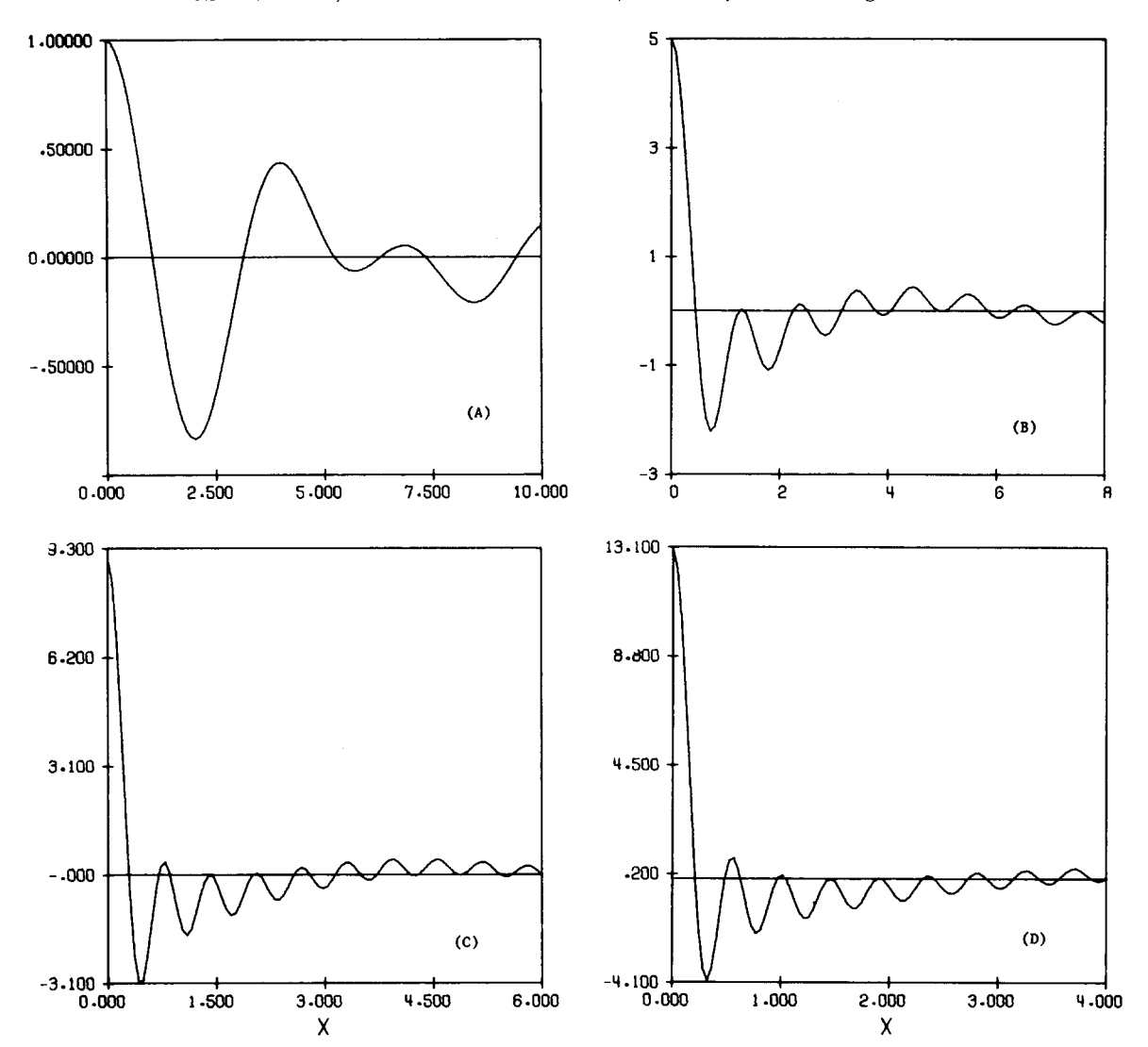


Fig. 9. Function  $\Delta(x)$  defined by Eq. (4.26) for  $k_- = 1$  and (A):  $k_+ = 2$ ; (B):  $k_+ = 6$ ; (C):  $k_+ = 10$ ; and (D):  $k_+ = 14$ .

On the plane  $\xi_3 = 0$ , Eq. (A.3) reduces to

$$\mathbf{u}' = A\boldsymbol{\alpha}(\phi_L) \exp(\mathrm{i}k_L \boldsymbol{p}^L \cdot \boldsymbol{\xi}) \tag{A.10}$$

where

$$\boldsymbol{\alpha}(\boldsymbol{\phi}_L) = \boldsymbol{p}^L + R_L^L(\boldsymbol{\phi}_L)\boldsymbol{p}^{Lr} + R_T^L(\boldsymbol{\phi}_T)\boldsymbol{d}^{Tr}. \tag{A.11}$$

# Acknowledgment

This work was carried out in the course of research sponsored by the Los Alamos Scientific Laboratory, under Contract N68-8539G-1 with Northwestern University.

The authors should like to acknowledge the contribution of H. McMaken and A.K. Gautesen to the result given by Eq. (4.6).

#### References

- [1] M.C. Brown, R.B. Duffield, C.L.B. Siciliano and M.C. Smith, *Hot Dry Rock Geothermal Energy Development Program (Annual Report 1978)*, LA-7807-HDR, Los Alamos Scientific Laboratory, Los Alamos, New Mexico (1978).
- [2] D.O. Thompson, Interdisciplinary Program for Quantitative Flaw Definition, Special Report Fourth Year Effort, Science Center, Rockwell International, Thousand Oaks, CA (1978).
- [3] J.D. Achenbach, A.K. Gautesen and H. McMaken, "Diffraction of point-source signals by a circular crack", Bull. Seism. Soc. Am. 68, 889 (1978).
- [4] J.D. Achenbach, A.K. Gautesen and H. McMaken, "Diffraction of elastic waves by cracks-analytical results", in: Y.H. Pao, ed., Elastic Waves and Non-Destructive Testing of Materials, AMD—Vol. 29, American Society of Mechanical Engineers (1978).
- [5] B.A. Budiansky and J.R. Rice, "An integral equation for dynamic elastic response of an isolated 3-D crack", Wave Motion 1, 187 (1979).
- [6] E.A. Kraut, "Review of theories of scattering of elastic waves by cracks", IEE Trans. Su-23, 162 (1976).
- [7] S.K. Datta, "Scattering of elastic waves", Mechanics Today 4 (1978).
- [8] Y.H. Pao and C.C. Mow, Diffraction of Elastic Waves and Dynamic Stress Concentrations, Crane Russak, New York (1973).
- [9] J.J. Bowman, T.B.A. Senior and P.L.E. Uslenghi, Electro-Magnetic and Acoustic Scattering by Simple Shapes, North-Holland, Amsterdam (1969).
- [10] Y.H. Pao (editor), Elastic Waves and Non-destructive Testing of Materials, AMD—Vol. 29, American Society of Mechanical Engineers (1978).
- [11] R.M. Lewis, "Physical optics inverse diffraction", IEEE Trans. Ant. Prop. AP-17, 308-314 (1969).
- [12] J.K. Cohen and N. Bleistein, "The singular function of a surface and physical optics inverse scattering", Wave Motion 1, 153 (1979).
- [13] H.P. Baltes (editor), Inverse Source Problems in Optics, Springer, Berlin (1978).
- [14] P.C. Sabatier (editor), Applied Inverse Problems, Lecture Notes in Physics No. 85, Springer, Berlin (1978).
- [15] J.D. Achenbach, Wave Propagation in Elastic Solids, North-Holland, Amsterdam (1973).
- [16] V.D. Kupradze, Dynamic Problems in Elasticity, Progress in Solid Mechanics, North-Holland, Amsterdam (1963).
- [17] E.F. Knott and T.B.A. Senior, "Equivalent currents for a ring discontinuity", IEEE Trans. Ant. Prop. AP-21, 693-695 (1973).
- [18] J.D. Achenbach, L. Adler, D. Kent Lewis and H. McMaken, "Diffraction of ultrasonic waves by penny-shaped cracks in metals: theory and experiment", J. Acoust. Soc. Am., to appear.